Hypoid Gear Vehicle Axle Efficiency

I. Kakavas[a,*], A. V. Olver[a], D. Dini[a]

[a]*Tribology Group, Department of Mechanical Engineering, Imperial College, London, UK*

Abstract

In this paper, a study of a hypoid gear vehicle axle is presented. Using a custom rig, load-independent losses have been accurately measured and the effect of viscosity on spin loss has been quantified. Solution methods for the calculation of component losses are presented and combined into a complete thermally-coupled transient model for the estimation of axle efficiency. An analysis of hypoid gear kinematics reveals a simplification, commonly adopted by other researchers, regarding the velocity of the point of contact in hypoid gears, to be in error. As a result, the calculation of lubrication parameters has been improved. Finally, experimental measurements are compared to the generated simulation results for a number of operating scenarios and satisfactory correlation is observed.

Keywords: Elastohydrodynamics, Lubrication, Friction, Contact mechanics, Hypoid gear

1. INTRODUCTION

The increasing global energy demand combined with environmental concerns, as well as the volatile value of crude oil[1] has driven governments and markets to pursuit higher efficiency in the automotive industry through incentives and legislation[2]. In the average passenger vehicle, around a third of the fuel is transformed into mechanical energy, while the rest escapes the system through high exhaust gas enthalpy and cooling. Although most of the mechanical energy consumption is utilised in overcoming driving resistances, a significant part is wasted in engine and transmission losses[3].

Transmissions and differential axles share the same core energy consuming components, i.e. gear pairs and rolling element bearings. Efficient powertrain design heavily depends on a thorough understanding of the operating behaviour of such components. Spur and helical gear pairs, common in vehicle gearboxes, have been extensively studied and a number of loss estimation methods have been proposed [4, 5, 6, 7, 8, 9]. In differential axles gear pairs with more complicated geometry, such as spiral bevel and hypoid gears, need to be used to achieve transmission of power through a right angle. Hypoid gears can offer higher load capacity and quiet operation for a small efficiency compromise, making them attractive to axle manufacturers[10]. On the downside, the complex geometry of hypoid gears has delayed the development of reliable tools for efficiency estimation tools. Recent work on hypoid gears involves contact models that require a great number of input parameters, extending to tooth cutting [11] or depending on separate

*Corresponding author. Tel.: +447413535162

Email address: i.n.kakavas@gmail.com (I. Kakavas)

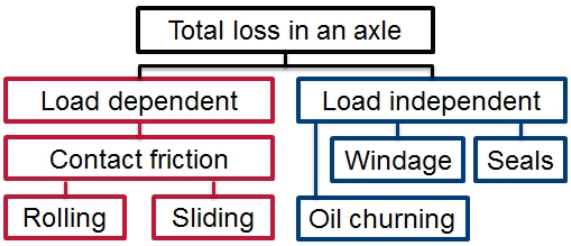

Figure 1: Axle losses categories

software packages [12]. In this study, hypoid gear vehicle axle losses have been quantified through experimental measurement and a simple axle efficiency estimation method is proposed.

2. EXPERIMENTAL SET-UP

The losses generated in a vehicle axle can be categorized as load-dependent or load-independent (Fig. 1). Load-dependent losses (e.g. those due to contact friction) arise when load is transferred in the contact of rough surfaces in relative motion and are the result of the interaction of lubricated rough surfaces[13]. In addition to the effect of load, the rolling and sliding velocities of the surfaces, as well as the lubrication regime, are defining parameters for the estimation of load-dependent losses. Load-independent losses (often referred to as spin losses) are mostly associated with fluid-surface interaction. More specifically, spin losses are the combination of oil churning and windage loss in the immersed revolving system and are not affected by contact loads[4]. Additional auxiliary losses (e.g. seal loss) are also included in the load-independent category.

The total axle losses as a function of torque and temperature may be measured, for example, using a dynamometer together with torquementers on input and output shafts. When no output torque is applied, the input

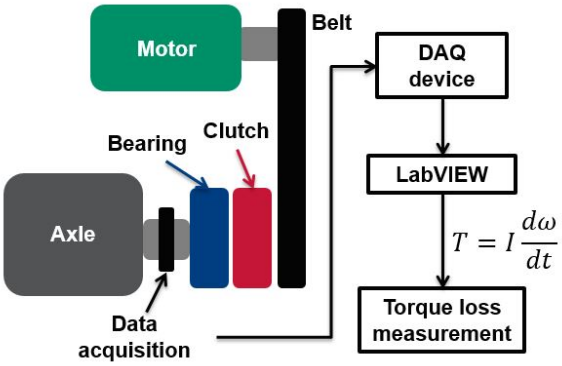

Figure 2: Methodology of spin loss measurement

torque may be too low for accurate measurement with a torquemeter. Here, a rig based on the inertia run-down method has been utilised (Fig. 2). The rig mainly consists of an electric motor, a clutch, an axle base and instrumentation. The axle is mounted on the base and connected to the electric motor through the clutch. By varying the power of the electric motor, the axle is accelerated to a desired speed. The clutch is then disengaged and the axle is allowed to decelerate naturally due to losses occurring in the rotating axle components. The rotational speed of the axle is constantly monitored using an optical encoder attached to the crown gear shaft. The captured rate of deceleration (d_ω/d_t) is then converted to instantaneous axle torque loss (T), given the rotational inertia of the axle (I). A flywheel has been attached to the input flange of the rear drive unit. This increases the total effective rotational moment of inertia to $I = 0.035\ kgm^2$ (referred to the high-speed shaft) prolonging the run-down period and serving to increase the time-resolution of the torque determination, particularly at low speeds. The differential gears of the axle were fixed with structural adhesive in order to ensure the two output shafts were synchronised.

In order to identify the relationship between viscosity and axle loss generation, lubricants

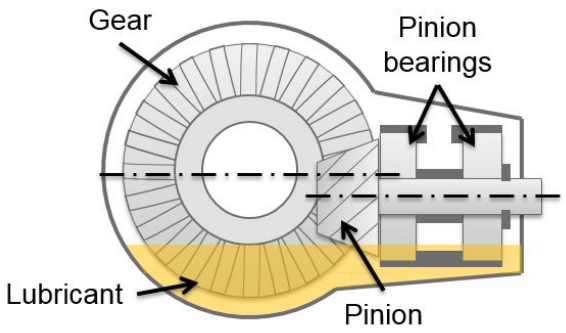

Figure 3: Axle section

of different viscosity (but with the same chemical additive package and base-stock type) have been used. The temperature of the oil sump is monitored prior to run-down initiation. In each case, standard production oil volume has been used allowing all four bearings and lower gear teeth to be sufficiently immersed (Fig. 3). The starting speed of the run-down was set to 2000 rev/min. Measurements were also conducted for 1000 and 500 rev/min in order to identify potential differences due to flow behaviour. Each test was run several (3-4) times to establish repeatability and a sixth-order polynomial is produced from the average values (Fig. 4).

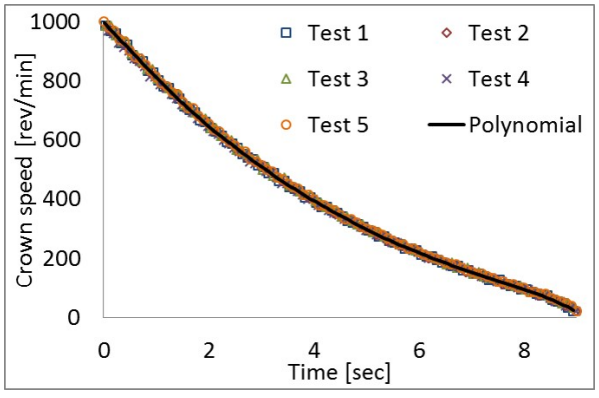

Figure 4: Crown gear speed data during a rundown

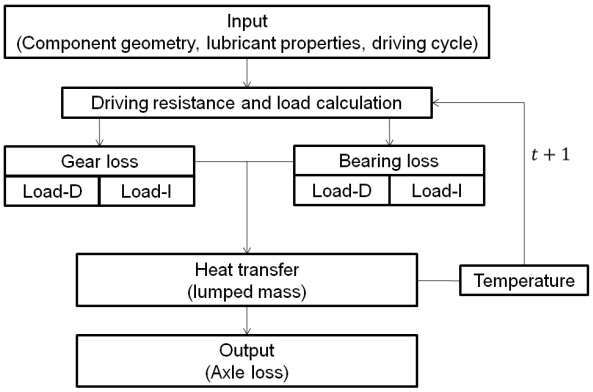

Figure 5: Transient axle simulation model algorithm

3. AXLE SIMULATION

3.1. Transient model

As displayed in Figure 5, the basic structure of the model consists of the initial parameter input, the theoretical component loss estimation, the heat transfer calculation and, finally, the axle loss/efficiency output. The transient component of the algorithm can be adjusted based on a specific drive cycle or any other time dependent input.

Apart from the calculation of the main component losses generation, all other parts of the model are relatively straightforward. There is no conventional way of calculating hypoid gear and bearing losses in the operating range of a passenger vehicle axle. Thus, the theoretical basis chosen for such a computational model will be described in the following sections, along with the assumptions adopted for the realisation of this model.

3.2. Driving resistance and load

The driving resistance opposing the motion of a vehicle is a function of the vehicle's speed[14] and other design constants (Eq. 1).

$$F_{resistance} = F_{drag} + F_{rolling} + F_{gradient} = 0.5\rho u_{veh}^2 C_D A + mgC_{rolling} + mg\sin\theta \quad (1)$$

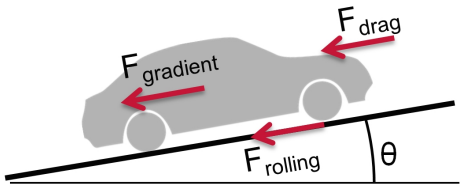

Figure 6: Vehicle driving resistance

Where ρ is the density of the air, u is the speed of the vehicle, C_D is the coefficient of drag (typically around 0.3), A is the frontal vehicle area, m is the mass of the vehicle, g is the gravitational acceleration and, finally, $C_{rolling}$ is the rolling friction coefficient (assumed to be equal to 0.015).

The force (F_a) needed to increase the speed of a vehicle over a given time is equal to the vehicle mass times the acceleration (du/dt) multiplied by a factor accounting for the rotating component inertia (k_m, typically between 1.08 and 1.1 [15])(Eq. 2).

$$F_a = k_m m \frac{du_{veh}}{dt} \tag{2}$$

The torque transmitted through an axle to overcome all opposing forces can be derived by Equation 3, given the wheel radius (R_{wheel}).

$$T_{transmitted} = (F_{resistance} + F_a) R_{wheel} \tag{3}$$

The resulting axial and radial loads on the teeth of the hypoid gear pair are given, for example, by Harris[16] based on the design angles of the gears.

3.3. Gear loss

3.3.1. Load-dependent

The load-dependent power dissipated in the gear mesh (P_{mesh}) is equal to the frictional force developed in the contact of the gear teeth ($F_{frictional}$) times the sliding velocity of the contact (u_s) (Eq. 4).

$$P_{mesh} = F_{frictional} u_s = \mu F_{load} u_s \tag{4}$$

Transient loading and local geometry/film thickness, although vital to durability, do not greatly affect mean power loss. As a result, average values for the parameters in Eq. 4 are used. Given the transmitted load, an estimation method for the friction coefficient (μ), as well as an analysis on hypoid gear kinematics are necessary for the calculation of the load-dependent power loss.

Gear kinematics

In order to analyse the lubrication of gear teeth, it is necessary to find the entrainment velocity ($\mathbf{u_e}$). This is defined[17] as the mean speed of the contacting (gear and pinion) tooth surfaces, relative to their point of contact. It represents the average speed at which the surfaces sweep the lubricant into the region of contact and hence controls their lubrication. $\mathbf{u_e}$ may be defined as:

$$\mathbf{u_e} \equiv \frac{1}{2}[(\mathbf{v_g} - \mathbf{v_c}) + (\mathbf{v_p} - \mathbf{v_c})] = \frac{1}{2}[\mathbf{u_g} + \mathbf{u_p}] - \mathbf{u_c} \tag{5}$$

Here, the suffices g and p indicate the actual surfaces of the pinion and gear and $\mathbf{u}$ indicates the component in the tangent plane of the velocities, $\mathbf{v}$. The corresponding normal velocities $\mathbf{n_g}$, $\mathbf{n_p}$ and $\mathbf{n_c}$ (Fig. 7) are identically equal and hence cancel from the above expression.

$\mathbf{u_c}$ is the velocity of the point of contact itself. In Equation 5, it is subtracted from each of the actual surface velocities to yield the required velocity relative to that of the point of contact.

A number of previous workers[18, 19] have made the additional assumption that $\mathbf{u_c}$ is zero so that Equation 5 becomes:

$$\mathbf{u_e} = \frac{1}{2}[\mathbf{u_g} + \mathbf{u_p}] \tag{6}$$

This assumption has probably been adopted due to the analysis being an extension of spur gear kinematics. In spur and helical gears, the

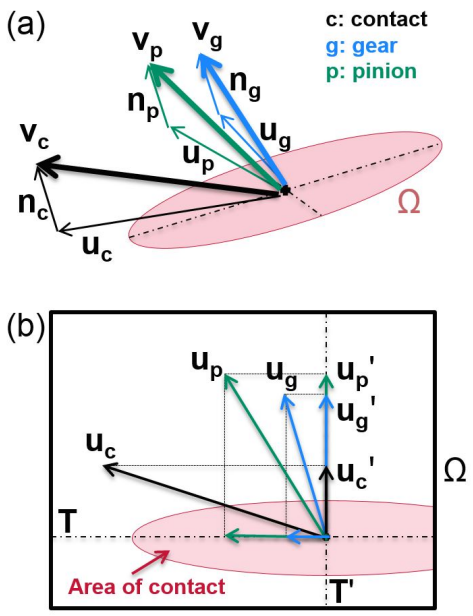

Figure 7: (a) Hypoid gear kinematic analysis, (b) Projection on tangent plane of tooth contact, Ω

point of contact moves in a straight line normal to the tooth surfaces. Hence its velocity is always normal to the tangent plane; the tangential component, ($\mathbf{u_c}$) is indeed zero and need not be considered. However, it is not apparent that this is correct for hypoid gears and it is certainly not true in the general case. Counter-examples include rolling bearings, where the points of contact orbit the assembly with the rolling elements and hence have velocities that are entirely tangential and cams and tappets, where the contact typically oscillates back and forth.

In addition, in the present work, we have considered only the component of $\mathbf{u_e}$ perpendicular to the major axis of the static area of contact ($\mathbf{T}$), thus the component on $\mathbf{T}'$ (Fig. 7). This is justifiable since entrainment parallel to the elongated contact has little effect on the lubrication. This is equivalent to adopting a line contact approximation.

In order to investigate the influence of velocity of the point of contact more extensively,

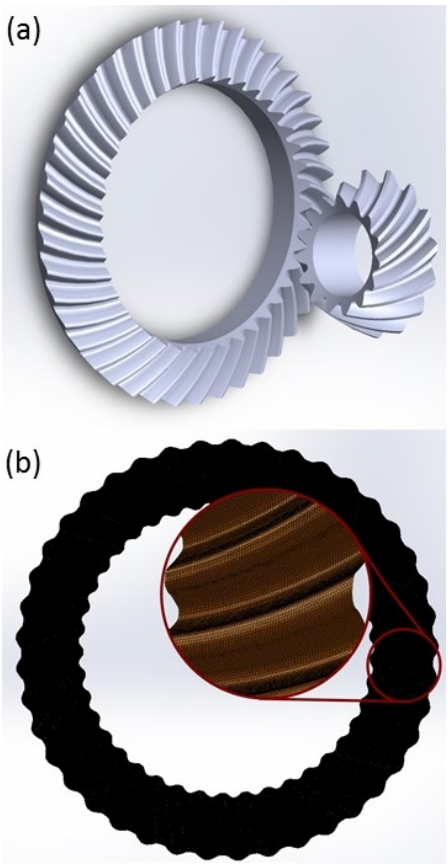

Figure 8: (a) CAD model of gear pair, (b) Dense polygon mesh on hypoid gear tooth surface

a rigid tooth contact analysis method was developed. First, a hypoid gear pair 3D model was designed (Fig. 8a) and the components were meshed based on high node density characteristics (element size = 0.5mm) (Fig. 8b).

Then, the node coordinates of the 3D parts were exported into Matlab and a program was created to solve for relative node distance between components. Tooth contact was detected by applying a predefined value of proximity as a filter. As a result, the component surface velocities and the velocity of the point of contact were calculated. A rigid surface was used and elasticity effects were not considered. This method accounts for completely general geometry and does not assume theoretical line contact or any particular solution of the law of

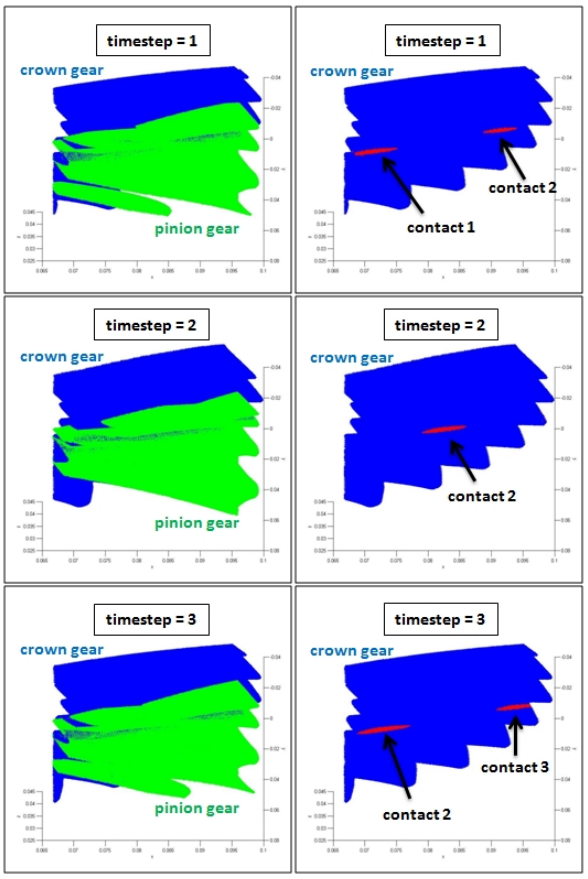

Figure 9: Progression of the rotation of the gears (LEFT) and the teeth pairs contacts (RIGHT)

gearing.

As the gears rotate, different nodes are found within a predefined distance of each other. In Figure 9, the rotation of the gear mesh can be observed along with the resulting contact area (red). On the first timestep displayed, two pairs of teeth are in contact. Subsequently, contact pair 1 goes out of proximity and only contact pair 2 continues. On the next timestep, pair 2 is closer to the end of its load sharing trajectory, while a third contact pair comes into contact. In Figure 10 it is possible to follow the contact of one pair of gear teeth from start to finish, displayed along the crown gear nodes in rotation.

With the node coordinates at each timestep

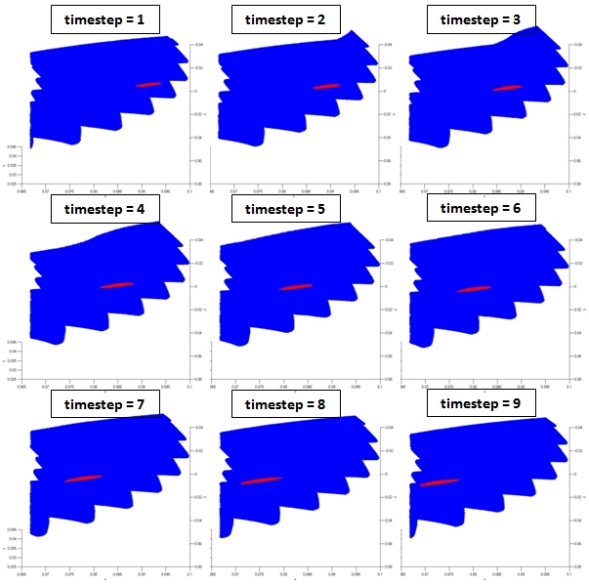

Figure 10: Progression of a contact as the crown gear rotates

available, the calculation of the tooth surface and point of contact velocities is possible. As seen in Figures 9 and 10, the progressing contact seems to be at a small angle to the tooth, as other researchers have predicted. However, it was found that the velocity of the point of contact ($\mathbf{u_c}$) is not normal to the contact plane for the hypoid gear in this application and, as a result, needs to be considered when estimating the entrainment velocity. Figure 7 shows these vectors approximately to scale for a typical contact position. Thus, the correct definition of the entrainment velocity is given by Equation 7:

$$\mathbf{u_e} = \frac{1}{2}[\mathbf{u_g} + \mathbf{u_p}] - \mathbf{u_c} \tag{7}$$

The entrainment speed and sliding velocities calculated in the contacts of the present hypoid gear pair model produced an average slide-to-roll ratio of the order of 70%. Based on the definition of average entrainment speed distributed along the tooth contact profile in other relevant work on hypoid gears [20], u_e

can be written as a function of ω and an effective radius (R_e) that depends on geometry (Eq. 8). For the hypoid gear set in this project, R_e is found to be approximately $1/3$ of the pitch radius of the gear:

$$u_e = \omega R_e = \omega 0.34 R_{pitch} \tag{8}$$

Furthermore, the velocity of the point of contact normal to the contact plane ($\mathbf{n_c}$) was found to be equal to the corresponding gear and pinion velocities ($\mathbf{n_{g,p}}$), which confirms that the gears in this model are conjugate.

Friction coefficient

For the estimation of the gear friction coefficient, the method described by Olver and Spikes [21] has been utilised. This approach provides a simple semi-analytical predictive tool that has the potential to be useful for comparing designs and lubricants.

The method utilises a limited shear stress approach, previously developed by Johnson and others [22, 23, 24]. The friction coefficient of a contact (μ_f) is given by the mean shear stress ($\overline{\tau}$) over the mean pressure in the contact ($\overline{p}$) (Eq. 9). For $\overline{\tau}$ equal to the non-dimensional shear stress ($\overline{\tau}^*$) times the Eyring stress (τ_E), we define:

$$\mu_f = \frac{\overline{\tau}}{\overline{p}} = \frac{\overline{\tau}^* \tau_E}{\overline{p}} \tag{9}$$

The following non-dimensional values are defined (Eq. 10):

$$S = \frac{\dot{\gamma}\eta_0}{\tau_E}, \qquad D_0 = \frac{\eta_0 u_e}{2aG_e}, \qquad \tau_c^* = \frac{\tau_c}{\tau_E} \tag{10}$$

Here S is the non-dimensional strain rate and is a function of the strain rate ($\dot{\gamma}$), the dynamic viscosity (η_0) and the Eyring stress. The Deborah number (D_0) is a non-dimensional parameter used to characterise fluid elasticity. It is a function of dynamic viscosity, entrainment speed (u_e), the lubricant pressure-viscosity coefficient (a) and the elastic shear modulus (G_e). Finally, τ_c^* is the non-dimensional limiting shear stress, which is the limit that is employed when the shear rate exceeds the maximum for Newtonian behaviour, and is equal to the limiting shear stress (τ_c) over the Eyring stress.

In order to calculate the viscosity of the lubricant inside the contact (η_r) under pressure, the formula provided by Roelands [25] is adopted (Eq. 11).

$$\eta_r = \eta_0 e^{(\frac{p'a}{z}[(1+\frac{\overline{p}}{p'})^z - 1])} \tag{11}$$

Where η_0 is the lubricant viscosity at atmospheric pressure and p', z are constants taken as $1.9 * 10^8$ and 0.6 respectively.

Next, the mean shear stress formula depends on the values of the Deborah number and the non-dimensional strain rate. There are two criteria to determine the appropriate formula.

- Is the response viscoelastic? ($D_0 > 1$)
- Is there shear thinning? ($S > \sinh 1$)

Knowing the answer to those questions, the shear stress can be calculated using Table 1.

$S \leq \sinh 1$	
$D_0 \leq 1$	$\overline{\tau}^* = S$
$D_0 > 1$	$\overline{\tau}^* = S[1 - D_0(1 - e^{-1/D_0})]$
$S > \sinh 1$	
$D_0 \leq 1$	$\overline{\tau}^* = \sinh^{-1} S$
$D_0 > 1$	$\overline{\tau}^* \approx \ln(2S)1 - \ln(1 + 2\lvert S - \frac{1}{2}\rvert e^{-S/2D_0})$

Table 1: Mean shear stress determination

However, if the shear stress exceeds its limit

(Eq. 12):

$$\overline{\tau}^* > \tau_c^* \tag{12}$$

Then, it is taken as the limited value (Eq. 13):

$$\overline{\tau}^* = \tau_c^* = 0.06\overline{p}/\tau_E \tag{13}$$

For gears, a correction needs to be applied to the friction coefficient, to account for the cyclic variation of contact conditions, as well as, the effect of surface roughness. The suggested equation to fit μ to a gear pair includes experimental measurements of boundary friction, thus, making it more reliable (Eq. 14) .

$$\mu = \mu_f + \frac{\mu_b - \mu_f}{(1+\lambda)^m} \tag{14}$$

Where μ_f is the friction coefficient as calculated through the procedure described above, μ_b is the coefficient of boundary friction as measured from experiments, m is an exponent coefficient, and λ is the lambda ratio of the contact surfaces. Attempting to correlate the estimation of μ with previous friction measurements for similar operating conditions, it was found that the best fit occurs with $\mu_b = 0.12$ and $m = 7$.

3.3.2. Load-independent

A gear immersed in lubricant will displace oil while in operation. The energy consumed by this process is called the churning loss. After a number of experiments on a similar hypoid gear axle, Jeon [26] proposed a formula that best fitted his measurements of churning losses (Eq. 15 and 16).

$$T_{ch} = 0.5\rho_{lub}\omega^2 R_p^2 b S_m C_m \tag{15}$$

$$C_m = 10\left(\frac{h_{lub}}{R_p}\right)^{0.1786}\left(\frac{V_{lub}}{R_p^3}\right)^{-0.2195} Re^{-04169} Fr^{-0.4482}\left(\frac{\nu_{lub}}{\nu_{air}}\right)^{-0.1777} \tag{16}$$

For the calculation of the churning torque (T_{ch}), parameters that are taken into account include lubricant immersion (h_{lub}), gear geometry (gear pitch radius, R_p, thickness, b, immersed area, S_m), the viscosities of the lubricant (ν_{lub}) and air (ν_{air}), as well as operating parameters such as contact/lubricant kinematics represented by the Reynolds (R_e) and Froude numbers (Fr) and the rotational speed of the gear (ω).

3.4. Bearing loss

The amount of loss generated by the supporting bearings can be calculated using the empirical method developed by SKF[27].

$$M = \phi_{ish}\phi_{rs}M_{rr} + M_{sl} + M_{seal} + M_{drag} \tag{17}$$

As seen in Equation 17, the total frictional moment (M) of each bearing is given as a function of rolling friction ($M_(rr)$), sliding friction (M_{sl}), seal friction (M_{seal}), and oil drag (M_{drag}). The effects of shear heating (ϕ_{ish}) and starvation (ϕ_{rs}) on rolling friction are also accounted for.

3.5. Thermal model

While friction and churning inside the axle generate heat and increase the temperature of the components, air convection on the housing of the axle, occurring on a moving vehicle, is cooling the system down. Heat transfer needs to be calculated for the prediction of the loss profile of a transient system to be possible. In reality, temperature varies across the mass of the axle. However, here we assume that the axle is at a uniform temperature identical to that of the oil supplied to the gear mesh. In order to calculate the external convective heat transfer coefficient, the shape of the axle is considered to be a cylinder of finite length. Adopting these simplifications,

the temperature after each iteration can be calculated.

If the lumped mass absorbed all the generated heat, then the temperature of the axle after one timestep would become (Eq. 18):

$$T_{t+1} = T_t + \frac{Q}{m_e C_p} \tag{18}$$

Here Q is the net heat generated in the axle within the timestep, m_e is the equivalent lumped mass of the axle, and C_p is the heat capacity of the equivalent mass.

Due to air flow on the axle housing, heat is transferred from the components to the air (Eq. 19).

$$Q_{convection} = hA_{axle}\Delta T \tag{19}$$

The heat transfer coefficient due to forced convection (h) can be calculated using Equation 20:

$$h = \frac{kNu}{D} \tag{20}$$

With Nu being the Nusselt number, D the characteristic length parameter of the shape within the flow, and k the thermal conductivity of the fluid which in this case is the environmental air.

For a cylinder of finite length the Nusselt number is given as a function of the Prandtl and Reynolds numbers from the Churchill-Bernstein equation [28] (Eq. 21):

$$Nu = 0.3 + \frac{0.62Re^{0.5}Pr^{1/3}}{(1+(\frac{0.4}{Pr})^{2/3})^{1/4}}[1+(\frac{Re}{282000})^{5/8}]^{4/5} \tag{21}$$

Where:

$$Pr = \frac{\nu}{a_t}, \qquad Re = \frac{uD}{\nu}$$

Here u is the velocity of the flow (taken equal to the speed of the vehicle), a_t the thermal diffusivity, D the characteristic dimension of the shape, and ν the kinematic viscosity.

Finally, the actual temperature of the axle (T^*_{t+1}) as a result of the effects of internal heat generation and forced convection within the duration of the chosen timestep is given by combining Equations 18 and 19 into 22:

$$T^*_{t+1} = T_{env} + e^{\frac{-hA_{axle}}{mC_p}dt}(T_{t+1} - T_{env}) \tag{22}$$

4. RESULTS

4.1. Spin loss measurements

Load-independent losses for a hypoid gear axle were measured using the experimental set up detailed in section 2. Initially, the axle deceleration was measured at four viscosity points as seen in Figure 11.

These measurements were repeated for three different starting speeds (2000, 1000 and 500 rev/min) and the generated data were converted to axle torque and power loss. Additionally, losses were estimated using the axle model proposed in Section 3. In Figure 12 the torque and power losses generated in the axle with different viscosity lubricant are presented along with the relevant prediction results.

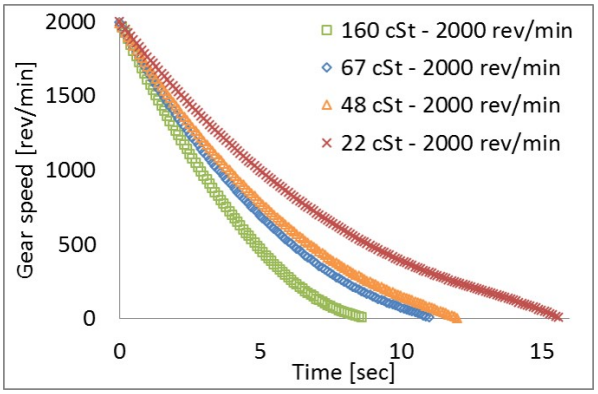

Figure 11: Axle deceleration data

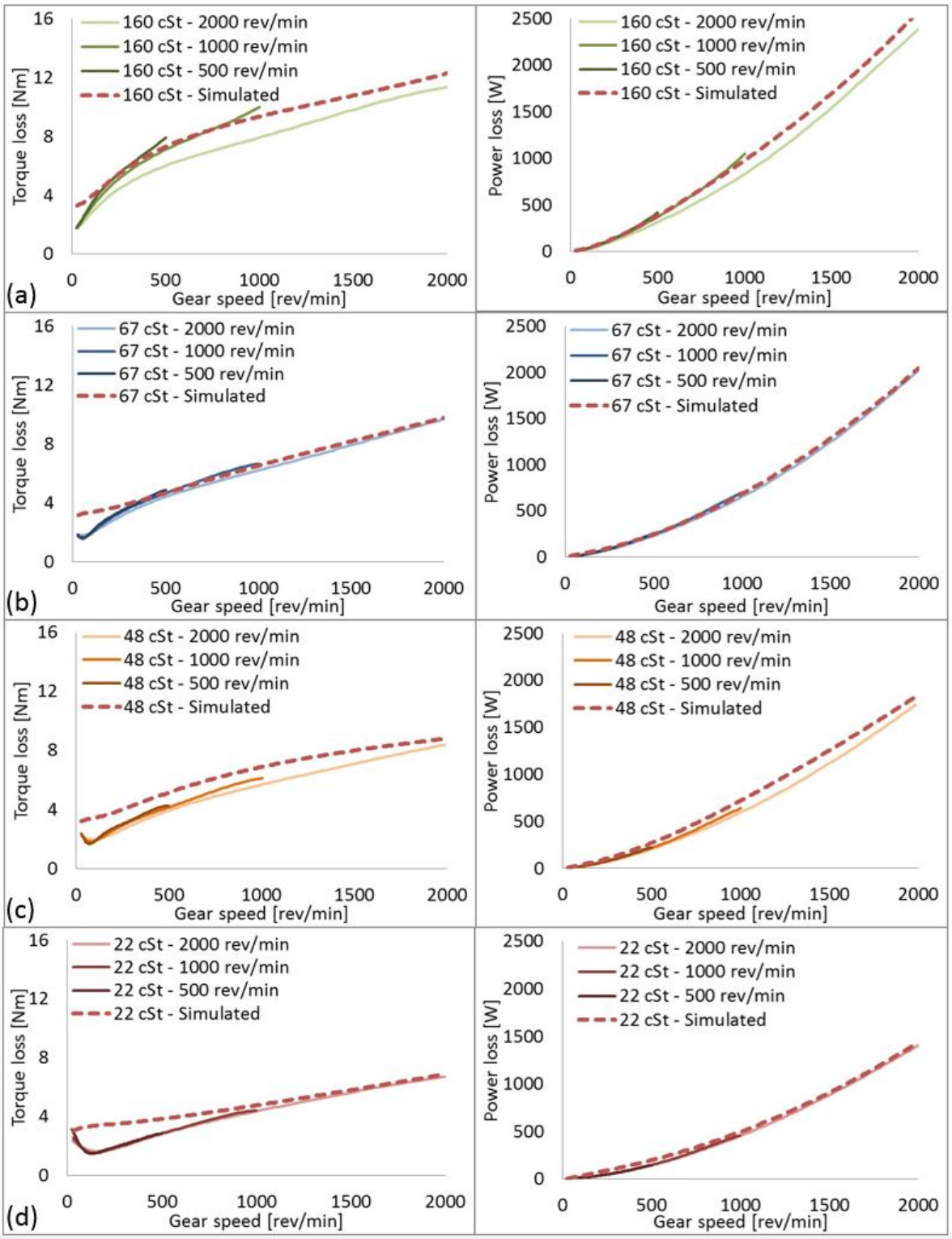

Figure 12: Correlation of predicted steady-state spin torque and power loss with run-down measurements at each of three different starting speeds. (a) lubricant A at 30 °C, (b) lubricant A at 50 °C, (c) lubricant B at 30 °C and (d) lubricant B at 50 °C

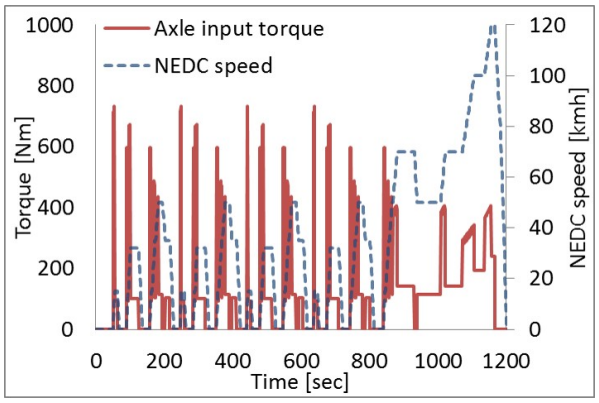

Figure 13: Axle input torque required for the present passenger vehicle over the NEDC

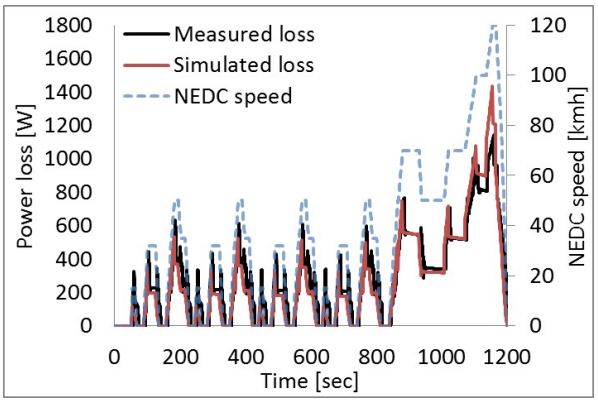

Figure 14: Axle power loss prediction compared with on-vehicle measurements over the NEDC

As seen in these graphs, the prediction correlates well with the spin loss measurements. However, at very low speeds, the model seems unable to fully capture the frictional behaviour of the axle. This is probably due to the fact that the transition to mixed lubrication is not explicitly modelled for the bearings. Nevertheless, the prediction of the rest of the speed range fits the measurements accurately and provides a useful design tool, especially considering the small contribution of loss under 200 rev/min.

4.2. NEDC simulation

The production axle utilised in this study had previously been tested on a vehicle, thus, loss and temperature measurements were available for the New European Drive Cycle (NEDC). This is a mild, mainly urban drive cycle on level terrain. Subsequently, the predictive model was used to simulate the drive cycle. The axle input torque required by the present vehicle over the NEDC is shown in Figure 13.

In Figure 14, the correlation between the simulation and the measured NEDC axle losses on the vehicle is shown. For the most part, losses are predicted accurately and follow the measured trends. At the highest speed however, there is up to 15% discrepancy, possibly due to the lumped mass thermal model being unable to account for rapid local temperature rises in the brief period of high speed in this drive cycle. Increasing the fidelity of the thermal model by mapping discrete areas of the axle could significantly improve correlation with measurements [29].

In Figure 15, the temperature progression of the lubricant sump from the probe in the tested axle is compared to the prediction obtained using the lumped mass thermal model. Again, the predicted temperature rise is within a few % with the largest discrepancy in rate of temperature rise at the end of the test where the speed is highest.

With the calculated overall axle loss providing good correlation to on-vehicle measurements, the individual component loss contribution can be estimated. As presented in Figure 16, bearing loss (contact friction and lubricant churning) dominates the overall axle loss over the NEDC. During steady speed intervals, gear friction and churning loss amount to a very small contribution. However, while the vehicle is accelerating, gear friction causes significant power losses due to the added inertial load. A greater proportion of gear losses would, of course be expected for a drive cycle

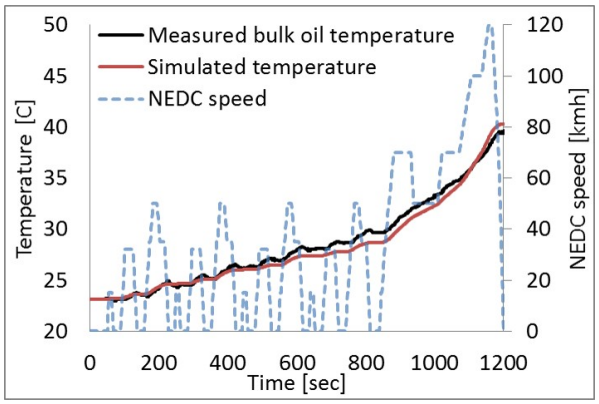

Figure 15: Axle lumped mass temperature prediction compared with bulk oil on-vehicle measurements over the NEDC

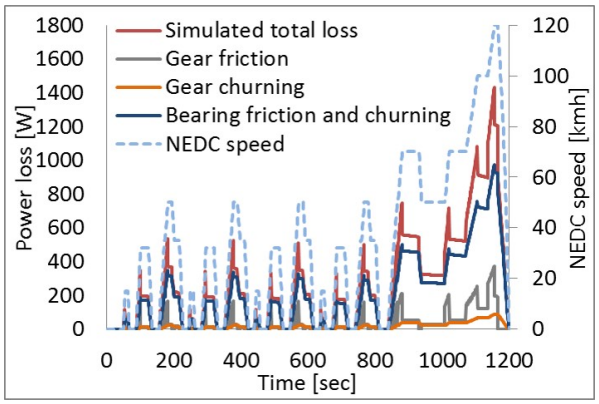

Figure 16: Breakdown of estimated axle loss over the NEDC for Axle lumped mass temperature prediction compared with bulk oil on-vehicle measurements over the NEDC

that included more severe (higher torque) conditions, such as high speed or inclined terrain.

5. CONCLUSIONS

A method to calculate hypoid gear axle efficiency has been presented, using a transient thermally coupled model of individual component losses estimation.

A kinematic analysis on hypoid gears has revealed a common misconception regarding the estimation of the entrainment speed in a hypoid gear tooth contact. A new definition has been proposed that accounts for the velocity of the point of contact and produces more accurate results. Furthermore, experimental data on axle losses has been generated utilising a custom in-house rig and used, along with available data on the performance of a passenger vehicle under the NEDC, to validate the model.

Satisfactory correlation between measurements and simulation has been achieved, allowing for the use of the proposed model with confidence. As expected, hypoid gear axle losses heavily depend on lubricant viscosity. Results show that component contribution to losses varies with acceleration, with bearings appearing as the dominant source of loss under the NEDC. This suggests that rebalancing the focus of component optimisation has the potential to introduce significant improvements in terms of efficiency in transmission systems based on hypoid gears.

References

[1] U.s. energy information administration, www.eia.gov.

[2] The international council on clean transportation, www.theicct.org.

[3] K. Holmberg, P. Andersson, A. Erdemir, Global energy consumption due to friction in passenger cars, Tribology International 47 (2012) 221–234.

[4] R. Boness, Churning losses of discs and gears running partially submerged in oil, in: Proc. ASME Int. Power Trans. Gearing Conf, Vol. 1, 1989, pp. 355–359.

[5] A. Terekhov, Hydraulic losses in gearboxes with oil immersion, Vestnik Mashinostroeniya 55 (5) (1975) 13–17.

[6] B.-R. Höhn, K. Michaelis, T. Vollmer, Thermal rating of gear drives: balance between power loss and heat dissipation, American Gear Manufacturers Association, 1996.

[7] T. T. Petry-Johnson, A. Kahraman, N. Anderson, D. Chase, An experimental investigation of spur gear efficiency, Journal of Mechanical Design 130 (2008) 062601.

[8] C. Changenet, P. Velex, A model for the prediction of churning losses in geared transmissionspreliminary results, Journal of Mechanical Design 129 (2007) 128.

[9] G. Koffel, F. Ville, C. Changenet, P. Velex, Investigations on the power losses and thermal effects in gear transmissions, Proceedings of the Institution of Mechanical Engineers, Part J: Journal of Engineering Tribology 223 (3) (2009) 469–479.

[10] V. Bhandari, Design of machine elements, Tata McGraw-Hill Education, 2010.

[11] M. Kolivand, A. Kahraman, A load distribution model for hypoid gears using ease-off topography and shell theory, Mechanism and Machine Theory 44 (10) (2009) 1848–1865.

[12] H. Xu, A. Kahraman, Prediction of friction-related power losses of hypoid gear pairs, Proceedings of the Institution of Mechanical Engineers, Part K: Journal of Multi-body Dynamics 221 (3) (2007) 387–400.

[13] K. Martin, A review of friction predictions in gear teeth, Wear 49 (2) (1978) 201–238.

[14] G. Lechner, H. Naunheimer, Automotive transmissions: fundamentals, selection, design and application, Springer Science & Business Media, 1999.

[15] I. Husain, M. S. Islam, Design, modeling and simulation of an electric vehicle system, Tech. rep., SAE Technical Paper (1999).

[16] T. Harris, N. K. Michael, Rolling bearing analysis (2 volume set).

[17] K. L. Johnson, K. L. Johnson, Contact mechanics, Cambridge university press, 1987.

[18] M. Kolivand, S. Li, A. Kahraman, Prediction of mechanical gear mesh efficiency of hypoid gear pairs, Mechanism and Machine Theory 45 (11) (2010) 1568–1582.

[19] M. Mohammadpour, S. Theodossiades, H. Rahnejat, Elastohydrodynamic lubrication of hypoid gear pairs at high loads, Proceedings of the Institution of Mechanical Engineers, Part J: Journal of Engineering Tribology (2012) 1350650111431027.

[20] A. S. Kolekar, A. V. Olver, A. E. Sworski, F. E. Lockwood, The efficiency of a hypoid axlea thermally coupled lubrication model, Tribology International 59 (2013) 203–209.

[21] A. Olver, H. Spikes, Prediction of traction in elastohydrodynamic lubrication, Proceedings of the Institution of Mechanical Engineers, Part J: Journal of Engineering Tribology 212 (5) (1998) 321–332.

[22] K. Johnson, J. Tevaarwerk, Shear behaviour of elastohydrodynamic oil films, Proceedings of the Royal Society of London. A. Mathematical and Physical Sciences 356 (1685) (1977) 215–236.

[23] C. Evans, K. Johnson, The rheological properties of elastohydrodynamic lubricants, Proceedings of the Institution of Mechanical Engineers, Part C: Journal of Mechanical Engineering Science 200 (5) (1986) 303–312.

[24] C. Evans, K. Johnson, Regimes of traction in elastohydrodynamic lubrication, Proceedings of the Institution of Mechanical Engineers, Part C: Journal of Mechanical Engineering Science 200 (5) (1986) 313–324.

[25] C. Roelands, Correlation aspects of the viscosity-temperature- pressure relationship of lubricating oils, Groningen A3 (4).

[26] S. I. Jeon, Improving efficiency in drive lines: an experimental study on churning losses in hypoid axle, Ph.D. thesis, Imperial College London (2010).

[27] S. Group, Catalogue 6000/i en.

[28] S. Churchill, M. Bernstein, A correlating equation for forced convection from gases and liquids to a circular cylinder in crossflow, Journal of Heat Transfer 99 (2) (1977) 300–306.

[29] H. Xu, A. Singh, D. Maddock, A. Kahraman, J. Hurley, Thermal mapping of an automotive rear drive axle, SAE International Journal of Engines 4 (1) (2011) 888–901.

NOTATION

A	Vehicle frontal area
A_{axle}	Axle frontal area
C_D	Coefficient of drag
C_p	Heat capacity
$C_{rolling}$	Coefficient of rolling friction
D_0	Deborah number
F_r	Froude number
G_e	Elastic shear modulus
Nu	Nusselt number
P_r	Prandtl number
R_e	Reynolds number
R_{pitch}	Pitch radius
S	Non-dimensional strain rate
S_m	Gear immersed area
T_t	Temperature of lumped mass at t
T_{ch}	Churning torque loss
T_{env}	Environmental temperature
$T_{transmitted}$	Transmitted torque
V_{lub}	Lubricant volume
a	Pressure-viscosity coefficient
a_t	Thermal diffusivity
b	Gear thickness
g	Gravitational acceleration
h	Heat transfer coefficient
h_{lub}	Lubricant immersion
k_m	Rotating component inertia factor
m_e	Axle equivalent lumped mass
$\mathbf{n_{g,p}}$	Gear or pinion velocity normal to the contact plane
$\overline{p}$	Mean pressure in contact
t	Time
$\mathbf{u'_c}$	Component of the velocity of the point of contact on the contact plane perpendicular the the line of contact
$\mathbf{u_e}$	Entrainment velocity
$\mathbf{u'_{g,p}}$	Component of the gear or pinion tooth velocity on the contact plane perpendicular the the line of contact
$\mathbf{u_{g,p}}$	Gear or pinion tooth velocity on the contact plane
$\mathbf{u_s}$	Sliding speed
u_{veh}	Vehicle speed
$\mathbf{v_{g,p}}$	Gear or pinion tooth velocity
Ω	Contact plane
$\dot{\gamma}$	Strain rate
η_0	Dynamic viscosity
λ	Lambda ratio
μ	Friction coefficient
μ_b	Coefficient of boundary friction
ν	Kinematic viscosity
ρ	Density
$\overline{\tau}$	Mean shear stress in contact
$\overline{\tau}^*$	Non-dimensional shear stress
τ_c	Limiting shear stress
τ_c^*	Non-dimensional limiting shear stress
τ_E	Eyring stress
ϕ_{ish}	Shear heating coefficient
ϕ_{rs}	Starvation coefficient
ω	Angular velocity